JGR Planets

RESEARCH ARTICLE

10.1029/2025JE009333

Special Collection:
The Lunar Trailblazer Mission Collection: Mission, Instruments, Data Analysis Plan

The Lunar Trailblazer Lunar Thermal Mapper Instrument

Neil E. Bowles[1], Bethany L. Ehlmann[2], Rory Evans[1], Tristram J. Warren[1], Henry H. Eshbaugh[1], Greg King[1], Waqas Mir[1], Namrah Habib[1], Katherine Shirley[1], Fraser Clarke[1], Cyril Bourgenot[3], Chris Howe[4], Keith Nowicki[1,5], Fiona H. M. Henderson[1], Christopher S. Edwards[5], Rachel L. Klima[6], Kerri Donaldson Hanna[7], Calina C. Seybold[8], Andrew T. Klesh[8], David R. Thompson[8], Elise Furlan[9], Elena Scire[9], Judy S. Adler[9], Nicholas Elkington[1], Aria Vitkova[1], Jon Temple[1], and Simon Woodward[4]

[1]Department of Physics, University of Oxford, Oxford, UK, [2]Division of Geological & Planetary Sciences, California Institute of Technology, Pasadena, CA, USA, [3]Durham University, NETPark Research Institute, Sedgefield, UK, [4]STFC RAL Space, Harwell, UK, [5]Northern Arizona University, Flagstaff, AZ, USA, [6]Johns Hopkins Applied Physics Laboratory, Laurel, MD, USA, [7]University of Central Florida, Orlando, FL, USA, [8]Jet Propulsion Laboratory, California Institute of Technology, Pasadena, CA, USA, [9]California Institute of Technology/IPAC, Pasadena, CA, USA

Key Points:

- The Lunar Thermal Mapper (LTM) instrument will measure thermal infrared radiation from the Moon across from 400 K to <110 K
- The LTM instrument completed assembly, testing, calibration and integration on the Lunar Trailblazer spacecraft
- The LTM instrument demonstrated sensitives of <0.1 K at 400 K and <1 K at 110 K during ground testing and calibration

Correspondence to:
N. E. Bowles,
neil.bowles@physics.ox.ac.uk

Citation:
Bowles, N. E., Ehlmann, B. L., Evans, R., Warren, T. J., Eshbaugh, H. H., King, G., et al. (2026). The lunar trailblazer lunar thermal mapper instrument. *Journal of Geophysical Research: Planets*, *131*, e2025JE009333. https://doi.org/10.1029/2025JE009333

Received 2 OCT 2025
Accepted 29 APR 2026

Author Contributions:
Methodology: Nicholas Elkington
Software: Nicholas Elkington

Abstract

The Lunar Thermal Mapper (LTM) instrument is a UK Space Agency funded infrared radiometer designed and built for the National Aeronautics and Space Administration Lunar Trailblazer mission launched in February 2025. LTM is a pushbroom imaging filter radiometer with 15 channels that cover the wavelength range from 6.25 to 100 μm with a 40–70 m/pixel ground sampling. Lunar Trailblazer's mission is to understand the form, abundance and distribution of water across the lunar surface. LTM provides an independent measure of temperature to investigate thermal effects on water's mapped distribution as well as an independent measure of surface mineralogy. The LTM instrument's 15 infrared channels include four broadband temperature sensing channels (6.25–12.5, 12.5–25, 25–50 and 50–100 μm) plus 11 additional narrow band (~40 cm^{-1}) filters from ~7–10 μm to map and discriminate silicate composition. We review the LTM design and calibration campaign at the University of Oxford's Space Instrumentation facility and show that the instrument has sensitivity from 400 K with a Noise Equivalent Temperature Difference of <0.1 K to <1 K at 110 K for typical integration times (e.g., 30 Hz readout) from a nominal 70–130 km lunar orbit design altitude.

Plain Language Summary

This paper describes the Lunar Thermal Mapper instrument for NASA's Lunar Trailblazer mission. Lunar Thermal Mapper is a thermal imaging system designed to sense the temperature and composition of the lunar surface using the thermal infrared. By sensing the temperature environment of the Moon, Lunar Thermal Mapper supports the Trailblazer's mission to map water on the lunar surface.

1. Introduction

Remote sensing measurements of the Moon's thermal emission (e.g., from 5–100 μm) contain a rich source of information on surface temperature, thermal inertia, roughness and composition (e.g., Bandfield et al., 2011; Greenhagen et al., 2010; Paige, Siegler, et al., 2010). Early ground-based measurements (e.g., Pettit & Nicholson, 1930 and spatially resolved measurements of Murray & Wildey, 1964) and surface thermal modeling (e.g., Jaeger & Harper, 1950) gave the first indications of a ~2 cm lunar surface layer with fine particulate low thermal conductivity regolith over a layer of more compacted/rocky material with variations in night time temperature that correlate with features such as the bright rays from craters (Murray & Wildey, 1964).

Due to strong absorption of the Earth's atmosphere at thermal infrared wavelengths, early spatially resolved measurements of composition were from balloon-borne observations (Murcray et al., 1970) that showed a prominent peak in emissivity near 8 μm, the Christiansen feature (CF), associated with Si-O stretching vibrations and dependent on compositional variations in silicate polymerization (e.g., Greenhagen et al., 2010; Salisbury et al., 1970).

Observations of the lunar surface from orbit and the surface expanded significantly with dedicated instruments, in situ measurements and returned samples (e.g., from the US Apollo and Soviet Luna missions and more recently Chinese Chang'e landers). The Apollo 17 Infrared Scanning Radiometer (ISR, Mendell & Low, 1974) used a single-element uncooled bolometer detector to measure the thermal emission from 1.2 to 70 μm for ~25% of the

lunar surface at a spatial resolution of <10 km. The ISR recorded temperatures in the range of 80–400 K (±2 K) and found populations of night-time higher temperature thermal anomalies ("hot spots") that were associated with ejecta from small and fresh impact craters (Mendell, 1976). The Clementine Long Wave IR (LWIR) camera measured the first 55–200 m spatial resolution data (Lawson et al., 2000) with a single IR channel centered at 8.75 μm. However, the LWIR had a minimum detectable temperature of ∼200 K, limiting its usefulness at the polar regions where temperatures of <100 K are possible in the permanently shaded regions (PSRs) at the lunar poles.

Currently, the most comprehensive global thermal-IR data set is from the Diviner Lunar Radiometer Experiment ("Diviner," Paige, Foote, et al., 2010) in lunar orbit as part of NASA's Lunar Reconnaissance Orbiter (LRO) mission since 2009. Diviner has nine thermal infrared channels, with four (13–23, 25–41, 50–100, 100–400 μm) broadband channels for temperature sensing, two Solar channels for albedo determination and three narrow channels grouped near the 8 μm "Christiansen" feature to map surface composition at a spatial resolution of ∼320 × 160 m from LRO's original 50 km mapping orbit. Diviner has made global maps of surface thermal emission, mapping the full range of surface temperatures from <30 K in the PSRs at the north and south poles to >400 K at the equator (Paige, Siegler, et al., 2010). The compositional investigation based around the three 8 μm channels has shown the diversity of lunar lithologies, but with limitations due to only having three compositional spectral channels (Glotch et al., 2010; Greenhagen et al., 2010). Particularly for the most silicic and most mafic compositions, additional channels and wavelength range are needed to differentiate lithologies.

Diviner's long operational life (over 16 years as of this paper) has allowed significant re-processing of the data set, including seasonally constrained polar (>80° latitude) surface temperatures (Williams et al., 2019) that have provided important new constraints on possible volatile cold traps. These new results have increased the areas where temperatures of <110 K that can trap volatiles for >1 Gyr are greater (×2.8 and ×4.3 for south and north polar winter regions, respectively) relative to the initial results from Paige, Foote, et al., 2010. The potential area for water ice deposits was then further extended by Schorghofer et al. (2020), who used the Williams et al. (2019) re-analysis combined with thermodynamic modeling of the time-varying population of adsorbed water molecules on the lunar surface. This work showed that further ice trapping is also possible due to temperature driven vapor pumping that captures water ice below the surface.

Lunar Trailblazer carries a novel combination of two mapping instruments: the High-resolution Volatiles and Minerals Moon Mapper (HVM^3), a visible shortwave-infrared (VSWIR; 0.6–3.6 μm) imaging spectrometer that detects water and mineralogy (Ehlmann et al., 2025; Thompson et al., 2026), and the Lunar Thermal Mapper (LTM), a push-broom multi-spectral infrared imager designed to map temperature and mineralogical composition of the lunar surface in the thermal infrared (TIR, 6–100 μm). Critically, LTM provides information on how localized gradients in surface temperature affect lunar ice and OH/H_2O concentration.

The retrieval of accurate OH/H_2O spectral features on the Moon by remote sensing in the infrared is challenging due to the complex lunar thermal environment, especially at the subsolar point where surface temperatures can reach up to 400 K (Paige, Foote, et al., 2010). At high temperatures, thermal emission from the lunar surface contributes to the measured signal, complicating the quantification of water absorption features near 3 μm in the Moon Mineralogy Mapper (M^3) data that cutoff at 3 μm (Bandfield et al., 2018). Using the Deep Impact spectrometer, which measures longer wavelengths, an observation from existing data is that the 3 μm feature changes depth diurnally, at least in some terrains. In thermally corrected data, water absorptions are shallowest in the warmest times of day, suggesting that changes in surface temperature may drive off water, which returns in the lunar night (Laferriere et al., 2022; Sunshine et al., 2009). This migration of water on short timescales raises the prospect of a water cycle on the Moon. By contrast with the sunlit Moon, water is predicted to be stable in permanently shadowed regions (PSRs) at the poles that act as cold traps for volatiles (Zhang & Paige, 2009) and with sub-surface accumulation due to vapor pumping (e.g., Schorghofer et al., 2020). In other high-latitude regions, micro-cold traps have been proposed to occupy fractions of the lunar surface in shadowed regions of small craters and rocks because of >200 K temperature gradients between sun and shadow that could enhance sunlit regions' volatile-trapping potential (Hayne et al., 2021). NASA's Lunar Trailblazer mission, with its combined instruments measuring the visible to shortwave infrared and thermal infrared at the same time, is designed (Ehlmann et al., 2025) to address these questions, detecting and advancing our understanding of the form, distribution, abundance, and potential time-variation of water across the lunar surface.

Table 1
Lunar Thermal Mapper Instrument Summary

Item	Value	Description	Comments
Field of View (FOV), instantaneous Field of View (iFOV)	9° × 7°, 540 μrad	FOV and iFOV calculated with @7 μm diffraction limit with baseline detector	LTM detector is a 384 × 288 uncooled microbolometer array with 35 μm pitch
Spatial Sampling	40–70 m/px	Resolution of LTM on the lunar surface	Resolution will vary as a function of Lunar Trailblazer altitude, nominally 100 km ± 30 km
Detector f/number	1.5	f-number at the detector	Intermediate focus design
Spectral range:	6–100 μm	15 IR filters (see Table 1)	IR filters for temperature and compositional measurements
Spectral Resolution	15 spectral channels	11 narrow compositional channels, 4 broadband thermal channels	Individual spectral channels for temperature and composition mapping
Mass	4.5 kg		
Volume	225 × 265 × 110 mm	Including Multilayer Insulation Blanket	
Power	5 W average, 13 W peak		Peak power consumption during the pointing mirror rotation.

Here we describe the LTM measurement approach, and its investigation goals related to temperature and silicate mineralogy. We then describe the instrument and operations approach, followed by the data calibration pipeline.

2. LTM Measurement Approach and Investigation Goals

LTM measures surface-emitted thermal radiance in infrared wavelengths. The instrument is configured such that it measures in a pushbroom configuration for targeted observations from lunar orbit. LTM follows up on Diviner measurements of lunar surface temperatures and mapping of cold locations where long-term preservation of surface water ice is possible (Paige, Siegler, et al., 2010). A key question in understanding the form, abundance, and distribution of water on the Moon is understanding the effect of temperature on its mapped distribution. The LTM instrument addresses this issue by:

1. Providing simultaneous, independent lunar surface temperature maps of the same targets that HVM^3 observes for water mapping via four thermal infrared channels.
2. Providing higher spatial resolution, contiguous temperature maps (40–70 m/pixel) than existing data from Diviner aboard the Lunar Reconnaissance Orbiter.

LTM has been optimized to identify cold traps (<110 K) and measure surface temperatures (110–400 K, ±5 K), albeit with less accuracy in distinguishing the coldest temperatures (<110 K) that occur within permanently shadowed regions. To provide radiometrically accurate measurements, the LTM includes a pointing mirror that allows the instrument to view the lunar surface, an onboard blackbody target, and space as part of a typical observing sequence. The science team will then transform the counts-on-detector to surface-emitted radiance and then to surface temperature. LTM temperature data can then be directly related to the simultaneous measurements of water acquired by HVM^3 to understand the role of temperature and temperature variation in controlling water's form, abundance, and distribution, including any variation with lunar time-of-day.

LTM's main function is to provide an independent estimate of surface temperature to understand co-variance of water content with temperature. LTM's field-of-view overlaps with HVM^3's to capture the temperature of the surface contemporaneous with each HVM^3 observation. Because both instruments are operated simultaneously, LTM-measured surface temperature can be quantitatively correlated with local gradients in HVM^3-measured water concentration and search for small (<1 km) cold traps.

LTM also has a compositional investigation that expands on the highly successful Diviner Lunar Radiometer Experiment compositional investigation (Greenhagen et al., 2010; Paige, Foote, et al., 2010). While Diviner uses 3 channels to estimate the position of the Christiansen feature (CF), LTM has 11 narrow (~40 cm^{-1}) compositional channels from 7–10 μm (Table 2) These are sensitive to variations in silicate mineralogy, particularly the spectral region around the Christiansen feature emissivity maximum (e.g., Conel, 1969; Greenhagen et al., 2010). LTM's baseline set of infrared channels (Table 2) includes the three compositional channels that are part of the

Table 2
Lunar Thermal Mapper (LTM) Filter Bandpass Center Wavelengths, Filter Purpose, Filter Hardware Type and Diffraction Limited Size in μrad and LTM Pixels

#	Filter (μm)	Goal	Type	Effective IFoV diffraction limited (μrad)	Width in LTM pixels
1 (A1)	7	Composition Discrimination using the silicate feature. (narrow ~40 cm^{-1} channels)	Interference filter	540	1
2 (A2)	7.25			540	1
3 (A3)	7.5			540	1
4 (A4)	7.8			540	1
5 (A5)	8			540	1
6 (A6)	8.28			540	1
7 (A7)	8.55			540	1
8 (A8)	8.75			540	1
9 (A9)	9			540	1
10 (A10)	9.5			540	1
11 (A11)	10			540	1
12 (A12)	6.25–12.5 (A5)	Thermal		540	1
13 (A13)	12.5–25			610	2
14 (B1)	25–50		Mesh filter	1120	3
15 (B2)	50–100			2440	5

Note. Note that a non-diffraction limited LTM pixel has an IFOV of 540 μrad.

Diviner experiment. This will allow cross-calibration at the improved spatial resolution from Trailblazer's nominal 70–130 km operational orbit (~40–70 m/pixel for LTM and ~200 m for Diviner). The 11 channels were specifically chosen to better interrogate the position and characterize the shape of the entire Christiansen feature (CF, Figure 1) (see also Shirley et al., 2025). Radiance measured in these channels is converted to emissivity to provide coarse spectral information on composition. Quick-look parameter maps will also be delivered to highlight surface locations with spectral features of interest, such as the wavelength position of the Christiansen feature (Shirley et al., 2025).

Science targets for LTM's compositional investigation include:

1. The highly silicic constructs that were identified by their short (<7.8 μm) CF positions (e.g., Glotch et al., 2010; Jolliff et al., 2011) where LTM's spectral channels can be used to uniquely distinguish between quartz-, Na feldspar-, and K feldspar-rich lithologies.
2. Mg-spinel lithologies that occur in small (~<5 km) exposures in multiple geological settings (e.g., Pieters et al., 2014) where LTM's spectral channels can be used to estimate the plagioclase to spinel abundances.
3. Possible mantle exposures identified near impact basins where LTM can be used to examine the ratio of olivine to plagioclase (dunite vs. troctolite) (e.g., Arnold et al., 2016; Yamamoto et al., 2010).
4. Irregular Mare Patches with scales of 100–5,000 m where Trailblazer's higher spatial resolution will provide fully spatially resolved multi-spectral maps for the first time (e.g., Braden et al., 2014).

3. LTM Instrument and Operations

LTM (Figure 2, Table 1) builds on heritage from the Diviner Lunar Radiometer Experiment onboard the Lunar Reconnaissance Orbiter (LRO), the Mars Climate Sounder onboard the Mars Reconnaissance Orbiter, and the Earth-orbiting UKSA TechDemoSat-1 Compact Modular Sounder instrument.

3.1. LTM Subsystems and Components

LTM measures surface-emitted radiation using a novel five-mirror optical system and an uncooled micro-bolometer detector array to map the lunar surface (Figure 3). The filter assembly with the infrared filters and windows, mounted at an intermediate focus, divides the scene into 4 channels for temperature and 11 channels for

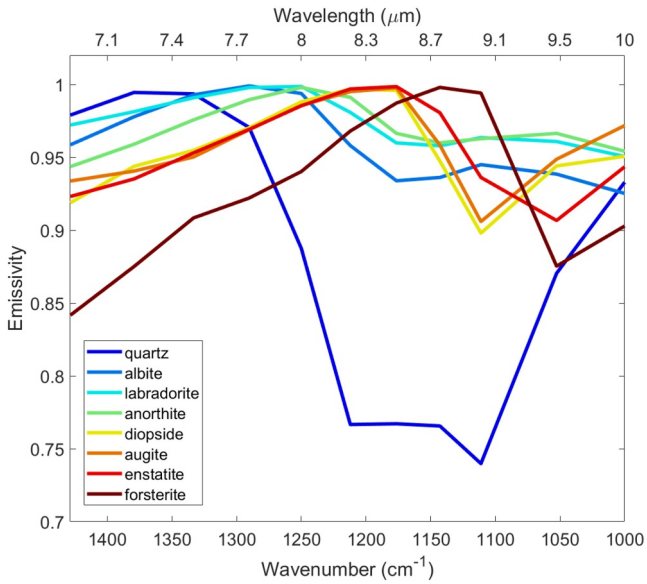

Figure 1. Relative emissivity of lunar analog minerals plotted using the Lunar Thermal Mapper compositional channel centers.

compositional mapping (6–100 μm; Table 2; Figure 4). The 15 filters were swept across the lunar surface in a push-broom fashion and re-imaged onto the 384 × 288-pixel uncooled microbolometer array.

LTM uses gold-coated all-reflective optics with f/1.5 at the detector and a 45-mm aperture. A two-mirror telescope directs the incoming infrared radiation onto the filter assembly. This filter assembly is then re-imaged onto an uncooled microbolometer array using a three-mirror relay. The placement of the filters at this intermediate focus is a critical part of the design because the magnification permits many channels to be included inside a small space volume and minimizes crosstalk between the channels from both thermal and optical effects. A black painted mask at one edge of the filter assembly that is ∼10 pixels wide at the detector prevents energy from the scene reaching the array. These obscured pixels then allow for characterization of stray light and thermal drifts that may occur between calibration cycles.

LTM's pointing mirror allows the instrument to view the lunar surface, an onboard blackbody target, and space. The cold-temperature space view gives a measurement of the calibration offset (zero), and the blackbody provides a known-temperature source of radiance to provide the instrument's gain. The blackbody target and space are viewed before and after each targeted observation of the lunar surface, allowing correction of temporal variation of the detector response over the measurement. Temperature changes in the detector and filter assembly between these calibrations are the limiting factor on LTM's absolute accuracy. The pointing mirror is capable of some limited Field of View (FOV) scanning, but this is not the baseline operating mode.

3.2. LTM Operation

3.2.1. Observation Sequence of Events

The Lunar Trailblazer (LTB) is described at a mission level in Ehlmann et al., 2025 (Section 6, this issue) and the spacecraft was planned to make at least one thousand targeted observations of the lunar surface during its nominal prime mission. For an observation, LTB acquires datacubes for both HVM3 and LTM instruments simultaneously with the spacecraft at 100 ± 30 km and oriented near-nadir such that data is obtained in a push-broom fashion with the instruments within a few degrees of nadir and with overlapping fields-of-view.

The baseline operations for the LTM instrument consist of sequences of multispectral image cubes of the lunar surface with space and calibration target views between surface observations. The instrument can be operated in either a “full frame” mode where all pixels from the microbolometer array are returned or by co-adding columns of pixels in each filter using a time-delay integration” (TDI) mode (Section 3.2.2). A standard observation sequence consists of the following steps:

1. Stabilize detector temperature using an optional thermo-electric cooler mounted on the detector
2. Average onboard calibration target views (nominally 32 TDI frames)
3. Move the pointing mirror to view space and average onboard space views (nominally 32 TDI frames)
4. Move the mirror to view the lunar surface and collect data via push-broom imaging (typically expected to take 10 s per observation with ∼500 TDI frames spanning 20–35 km along track at 40–70 m depending orbital altitude)
5. Move the mirror to view space and average onboard space views (nominally 32 TDI frames)
6. Move the mirror to view the calibration target and average onboard calibration views (nominally 32 TDI frames)
7. Return to standby mode

The uncalibrated data in counts are then transferred from the LTM's local instrument storage to the main LTB onboard computer for downlink. When not taking data, the LTM will remain in standby mode with the mirror in its safe position viewing the calibration target.

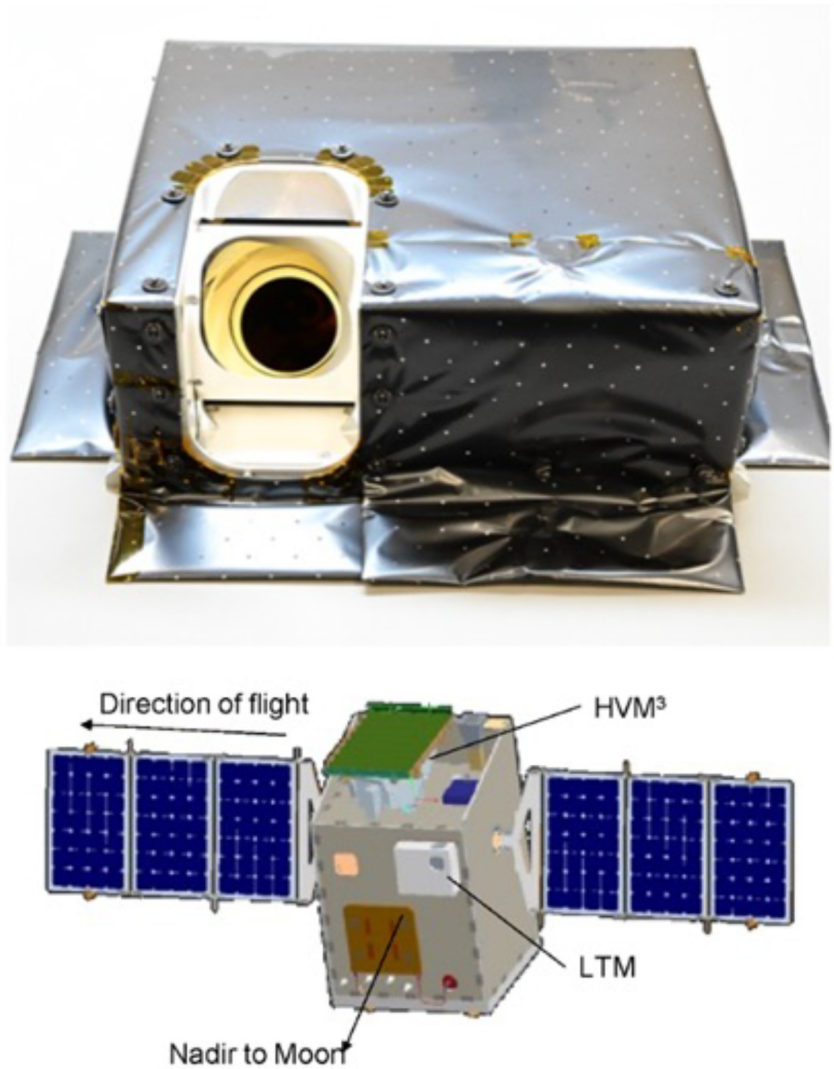

Figure 2. The Lunar Thermal Mapper (LTM) flight model before integration on the Lunar Trailblazer spacecraft and the position of the instrument on the spacecraft. The LTM instrument (top) is 225 × 265 × 110 mm including its multi-layer insulation blanket and 4.5 kg in mass. The Lunar Trailblazer spacecraft is approximately 200 kg and has a width of ~3.5 m with the solar arrays deployed.

The same detector setup parameters (e.g., integration time, TDI mode) are used for calibration and scene views. The range of integration times envisaged for the TDI mode in lunar orbit is 20–50 ms for line readout.

3.2.2. Time-Delay Integration Mode

To improve signal to noise, especially in the narrow (~40 cm^{-1}) compositional bands, LTM's firmware includes the option to provide TDI, synchronized in rate with spacecraft motion, as each channel is push-broomed across the lunar surface (Figure 5). TDI will be the default mode for LTM and is performed internally in the instrument's firmware rather than in the detector.

The detector array is divided into strips for each IR channel, programmable up to 16 pixels/channel in along-track. Use of 12 pixel along-track is expected for nominal operations in flight to maximize signal while reducing crosstalk between channels.

As Lunar Trailblazer push-brooms across the target, each of the LTM along-track detector pixels comprising the channel passes over the same part of the scene in sequence. Thus, succeeding frames from the array include a

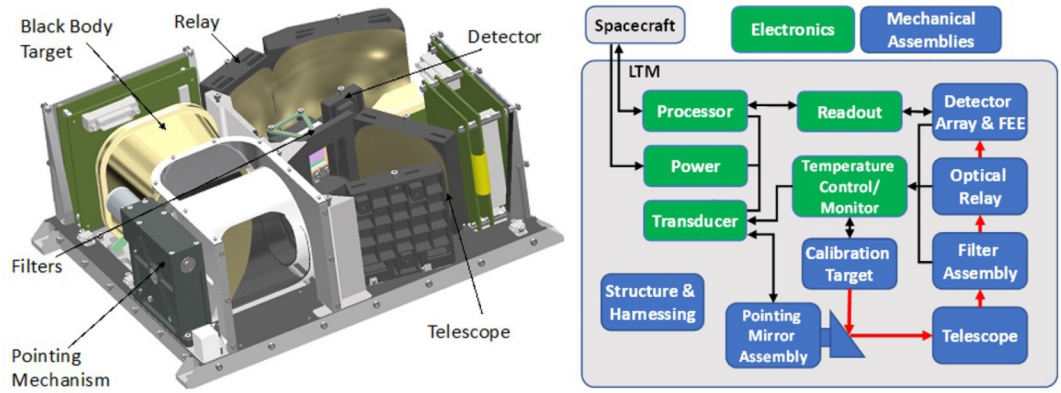

Figure 3. Lunar Thermal Mapper (LTM) instrument layout and block diagram. The CAD render shows the LTM instrument without its cover, showing the locations of the black body calibration target, optical elements and electronics.

different pixel viewing the same point on the surface. Each successive pixel that images the same spatial location within an LTM filter is stored in memory local to the detector array and co-added to increase the effective signal (Figures 5 and 6). The end downlinkable data product is 384 individual 16-bit pixels per each of the 15 channels cross-tracked. The length of the observation along-track is determined by the duration of the observation and sets the size that is stored and downlinked. TDI carried out onboard the instrument is not reversible on the ground.

When in TDI mode (Figures 5 and 6), the LTM instrument carries out the same internal process whilst viewing the calibration target and spaceview. This allows a gain and offset to be determined for each TDI-co-added pixel as part of the ground calibration pipeline.

Lunar Trailblazer has system-level requirements for alignment, jitter, timing, and position knowledge to ensure data quality from both instruments. TDI integration timing is controlled by an LTM instrument parameter prior to observation, based on the expected altitude and ground speed of the spacecraft. Any alignment and jitter errors would show in LTM data as imaging blurring and do not affect the radiometric calibration. Jitter (pitch, yaw, and roll) gives a 2-dimensional blur based on the amount of angular deviation during the observation and currently cannot be corrected. For off-nadir observation, there will be a horizontal blur of width.

$$\text{Horizontal blur} = n_{pix} * \tan(\text{roll Angle} + \text{distorion Factor})$$

where the distortion factor (in μrad) varies across the channels and accounts for geometric distortion of the optics slightly curving the projected along-track direction on the focal plane. For the example of 12 TDI pixels (n_{pix}), a 1° roll is ∼1/5 of an LTM pixel. The TDI settings will be optimized based on Lunar Trailblazer observation viewing geometries on-orbit.

3.2.3. Single Integration Mode

The TDI mode can be disabled and a single row of 384 pixels is output without TDI averaging. The row of 384 cross-track pixels used within a channel is selectable prior to the start of the observation. The output raw data format is the same as with TDI, 384 16-bit ADC values per channel representing the number of pixels in a cross-track measurement.

4. Instrument Testing, Characterization and Calibration

The LTM instrument went through radiometric alignment testing with filter assembly and detector response measured prior to integration into the completed instrument. Spectral response in the integrated instrument was confirmed by radiometric performance testing. Full details of the ground test calibration campaign for LTM are given in Evans et al., 2024 and summarized here.

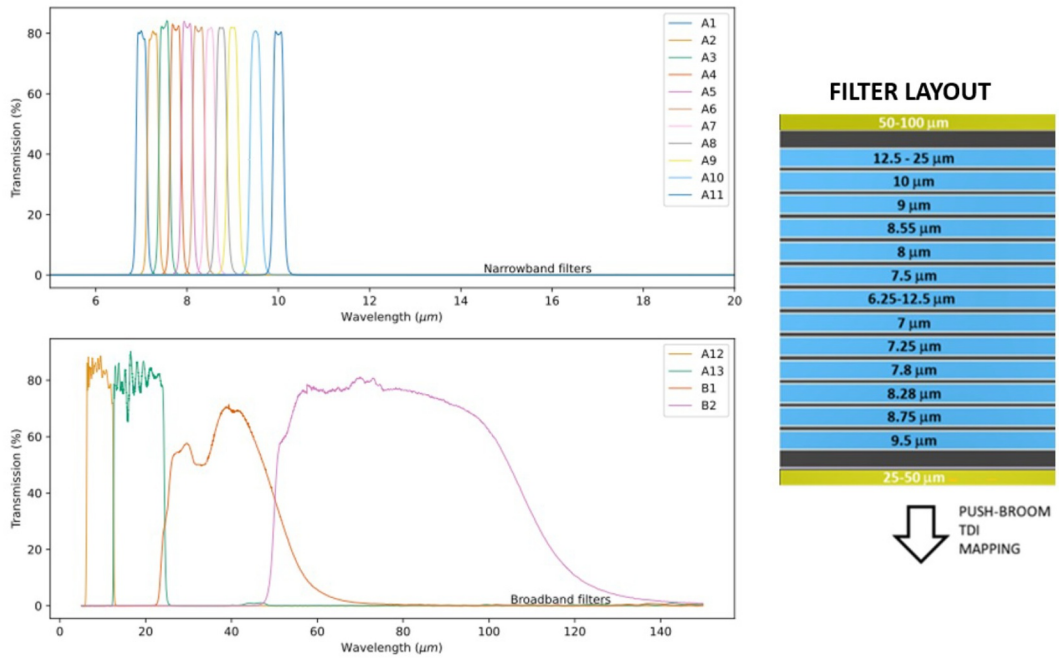

Figure 4. Lunar Thermal Mapper Compositional bandpass positions (top, left, Table 2), thermal broad bandpasses (bottom, left), and schematic layout of the physical filter configuration showing how they are push-broomed across the surface.

4.1. Ground Test Setup

4.1.1. Calibration Chamber Overview

The LTM calibration chamber design builds on the approach used for calibration of the Diviner Lunar radiometer (Paige, Foote, et al., 2010). The LTM calibration facility was installed in a clean room at the University of Oxford's space instruments laboratory and operated over 3-week period in February 2023. As shown in Figure 7, the instrument was mounted to a simulated spacecraft interface plate (at 290 K ± 0.1 K) within a cold shroud (<150 K). Using the LTM scan mirror, the instrument rotated the mirror between 4 views.

1. The internal calibration view and safe position as in flight.
2. A cooled black body target (<100 K) attached to a cold head was used for a high accuracy simulated space view.
3. A variable temperature black body target (100–400 K) was used as a high accuracy target for radiometric calibration.
4. A flip mirror to switch between views of a target projector and range of targets for geometric calibration, and a monochromator for end-to-end spectral calibration.

The interface is equivalent to the mechanical and thermal interface of the Lunar Trailblazer spacecraft, including PRT sensors and heaters to control the interface temperature <0.1 K. The cold shroud provides a small amount of radiative cooling to the spacecraft plate, which is sufficient to remove the excess heat from continuous operation of the LTM. A lunar simulator plate is also present to allow simulation of the out-of-field lunar thermal emission and can vary from 100 to 400 K.

The two external black body targets were used for radiometric calibration and to determine the linearity of the detector. Both targets were concentric grooved bases (60° opening angle) and painted with high emissivity paint (Nextel 82–11), with an integral baffle. The depth-to-diameter ratio of the targets are 1.5 and 1.7 for the cold and hot targets, respectively.

As can be seen in the cross-section view of Figure 8 and in Figure 9, the spacecraft simulator plate is mounted onto a gimbaled structure controlled by vacuum compatible motion stages. This structure allows the instrument to pan and tilt to move the view of the target projector and monochromator over the full FOV.

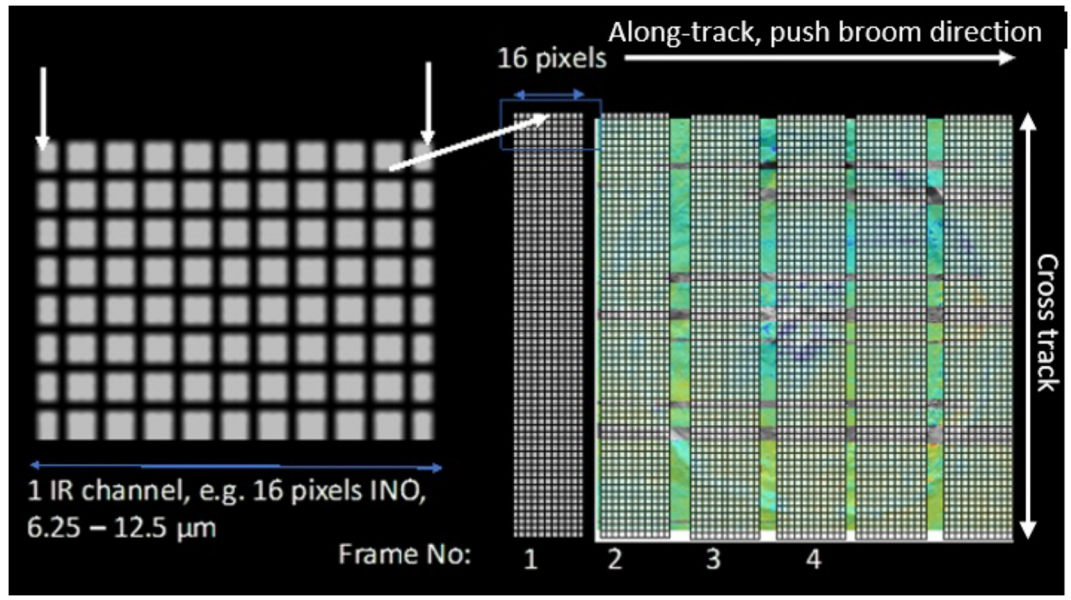

Figure 5. Illustration of time-delay integration for Lunar Thermal Mapper (LTM). A maximum case of 16 pixels is shown, 12 is used in normal operation. The diagram refers to the detector manufactured by the Institut National d'Optique, Canada (INO), who provided the gold black coated infrared detector array used in LTM.

The surfaces of the cold shroud and lunar simulator plate were all painted with high emissivity paint (Nextel 82–11). As seen in Figure 9 the exterior of these panels as well as the cold heads and thermal straps are covered with MLI blankets to isolate them from the chamber thermal emission and allow them to cool down to <150 K.

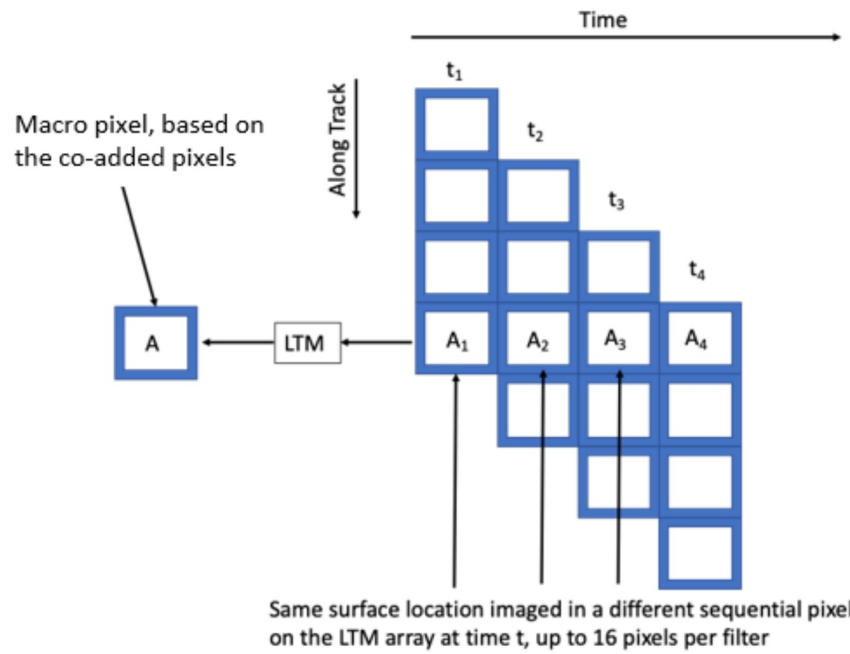

Figure 6. Example TDI observation sequence showing how an averaged macro-pixel is built-up as the Lunar Trailblazer spacecraft pushes brooms across the lunar surface. Only 4 pixels are shown for clarity. The standard operating mode for Lunar Thermal Mapper is co-adding of 12 pixels.

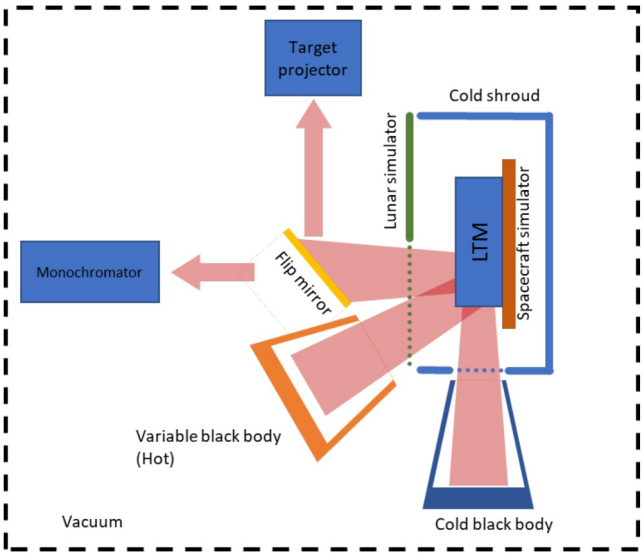

Figure 7. Calibration chamber generalized schematic showing the positions of the external blackbody calibration sources and geometric target projector.

4.2. Ground Test Campaign Overview

The LTM ground test campaign was carried out over a period of 3 weeks in February 2023. The calibration occurred in two runs split by instrument vibration and thermal vacuum (TVAC) environmental testing. Further details are in a manuscript in preparation by co-author R. Evans and are summarized briefly here.

The first run included radiometric calibration, during which the LTM instrument self-calibrates with an external simulated space view and then measures an external variable temperature black body. During this run, the black body was varied from 100 to 380 K and measured in multiple instrument modes using different detector integration time and gain settings. This provided an instrument functional check out and performance baseline for comparison post environmental testing.

The second calibration run was carried out after TVAC cycling and the instrument was put back into the calibration chamber for functional testing and geometric optical testing, with additional extended radiometric calibration repeated for a smaller range of set points from 200 to 350. The second run also included lessons learned from the pre-TVAC campaign, including updates to the instrument detector gain settings allowing fuller use of the instruments analog to digital convertor range, improving dynamic range.

The temperature of the calibration chamber during the second calibration run is shown in Figure 10. Two sets of calibration measurements were taken, one during continuous cooling of the variable target, and the second in 50K steps as the target heated.

4.3. Radiometric Accuracy

The ground test campaign (Section 4.2) showed that the measured performance exceeds LTM's level one requirements of <5 K precision (Figure 11).

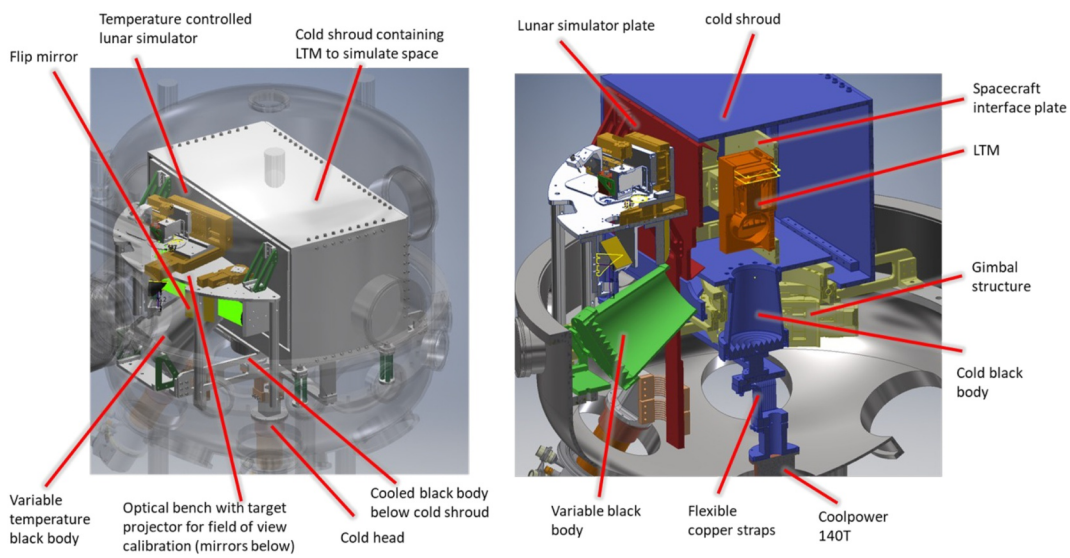

Figure 8. Calibration chamber CAD and cross-section view showing the positions of the external calibration targets, thermal environment shroud and mounting assemblies. The vacuum chamber is approximately 1 m in diameter.

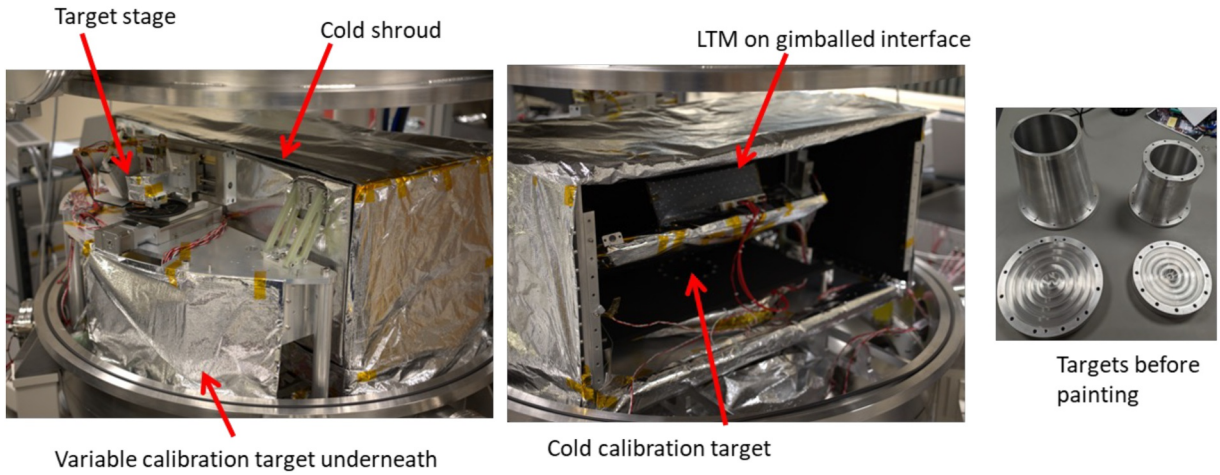

Figure 9. Assembled calibration chamber and calibration targets at the University of Oxford Space Instruments laboratory, February 2023 with the Lunar Thermal Mapper flight model installed on the gimbaled interface plate.

4.4. Detector Linearity

The linearity of the detector is determined from measurements of the external variable target black body. The measurements were carried out using two calibration runs that allowed investigation of the bolometer array's gain settings.

During the first run, the radiometric calibration target was stepped from 100 to 375 K in 25 K steps but with only limited adjustment of the detector's on-chip gain, thus reducing the overall range of data numbers digitized by the instrument's readout electronics. During the second calibration run, the calibration target was operated over a range of 200–350; however, due to the nature of the Plank function, this run still covered 75% of the instrument's operating range in radiance. For the second run, the detector's gain table was adjusted allowing operation at higher gain and allowing more coverage of the instrument's operation in flight. For this reason, the data measured during run 2 provided a better characterization of LTM's overall linearity.

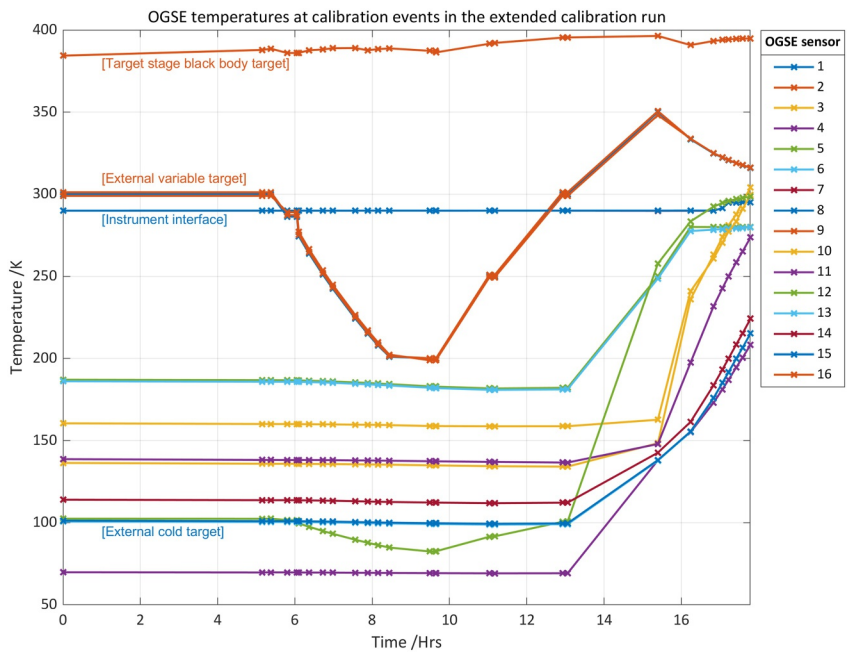

Figure 10. Optical Ground Support Equipment calibration chamber target temperature during calibration run 2.

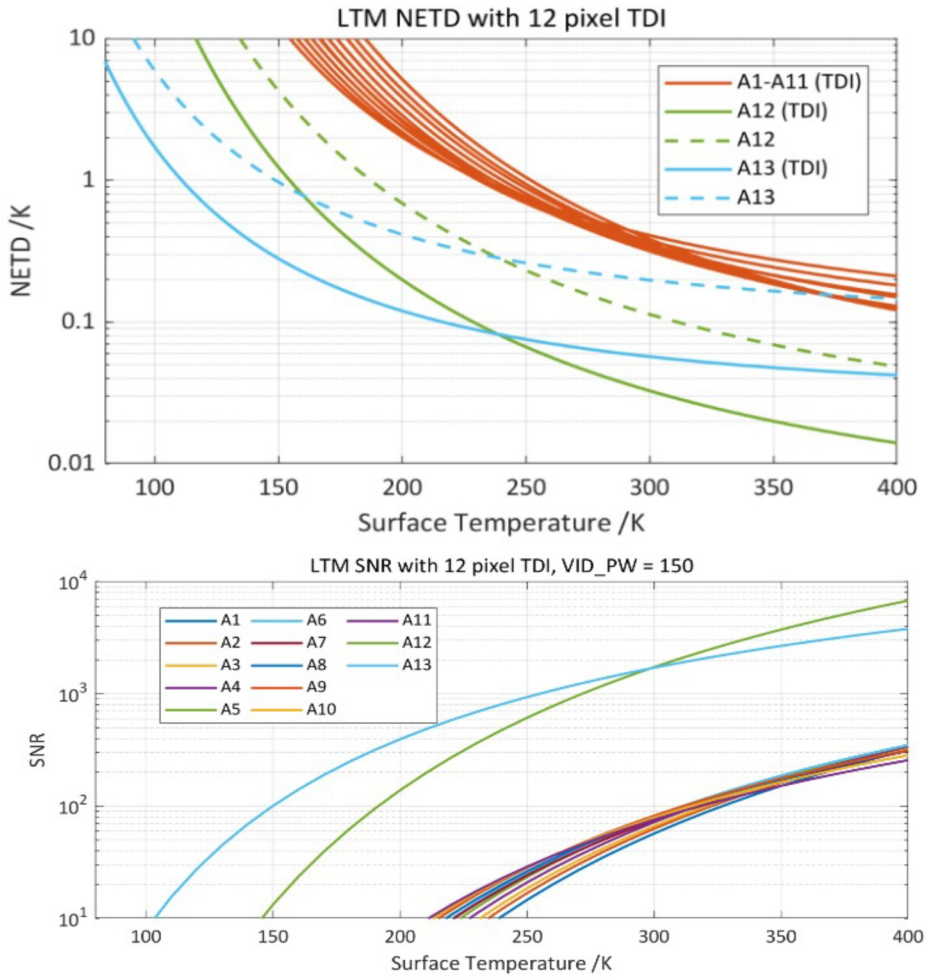

Figure 11. Lunar Thermal Mapper (LTM) radiometric performance was measured during the ground test calibration campaign. The NEDT (top) is the Noise Equivalent Temperature Difference, the difference in temperature for LTM that is equivalent to the instrument noise. This can also be represented as a Signal to Noise Ratio (SNR, bottom), showing the sensitivity of each of LTM's channels for different scene temperatures.

For each calibration, the radiance of the variable temperature target is determined within each channel following the calibration pipeline. The radiance of the target was also calculated using the PRT sensor temperature and LTM model for comparison. Plotting the measured radiance against the calculated target radiance will result in a 1:1 linear relationship for a well-calibrated instrument.

Linearity is evaluated using integral non-linearity (INL), defined as the maximum fractional error over the full scale. The microbolometer specification states a linearity of better than 5%. The linearity is plotted along with the calculated INL in Figure 12. Every channel performs better than the 5% quoted for the detector, with the slightly higher INL of the compositional channels predominantly caused by noise within the measurements at the low signal.

5. Radiometric Calibration Pipeline

After completing the observation at the Moon, the raw LTM science data from the Lunar Trailblazer spacecraft are provided as binary packets in CCSDS (Consultative Committee for Space Data Systems) format for downlink. Housekeeping data from the instrument are recorded by the spacecraft through its onboard data aggregator and reported separately.

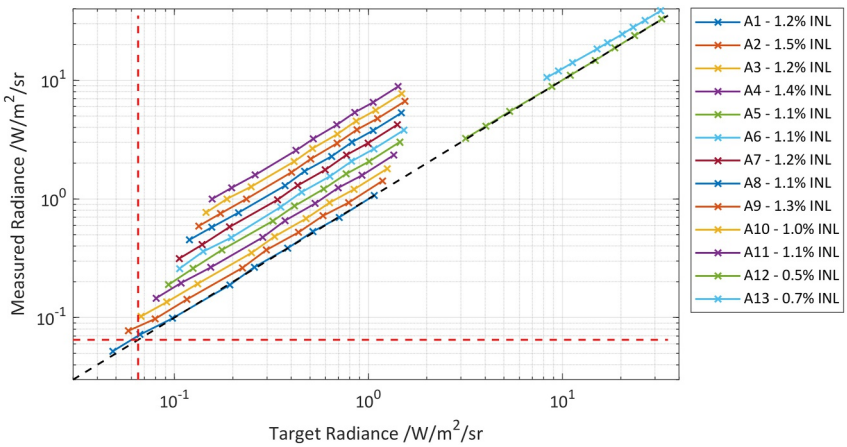

Figure 12. Detector Linearity, full range, channels are numbered and offset by a factor of 1.2 for each successive channel from A1. Red lines indicate the noise equivalent power, and INL is the Integral Non-Linearity.

The science data pipeline (Figure 13) is divided into two parts. The first unpacks the science data from LTM for a specific observation (referred to internally as an instrument timeline) that is tagged with metadata to allow calibration data, that is, the space and blackbody target views, and the lunar surface data in the instrument's internal flash memory to be associated with each other. The unpacked CCSDS packets are then stored for internal processing and converted to HDF5 format with the metadata used to tag calibration observations and instrument status (temperature, motor position etc.).

Once the HDF5 formatted files have been prepared, they are then passed to the science data system (SDS) where the data is processed using a series of calibration scripts. The calibration scripts, written in Python, are based on the ground test campaign processing and include steps for straylight removal, row/column and frame correction and detector pixel data number to radiance conversion using the tagged calibration views (Figure 14).

The calibrated per-pixel and per-channel radiance data are then ready for formatting into the correct format for delivery to the Planetary Data System as described in the Planetary Data System LTM Data User Guide and summarized below.

6. LTM Delivered Planetary Data System (PDS) Products

There are six primary LTM data products within four groups for delivery to the PDS:

RAW: Raw science data ("RAW") in units of digital counts.

RAD: Calibrated data in units of spectral radiance (W/m^2/str/μm) ("RAD"). Also includes ancillary files, pixel center location data (latitude, longitude), and observation geometry.

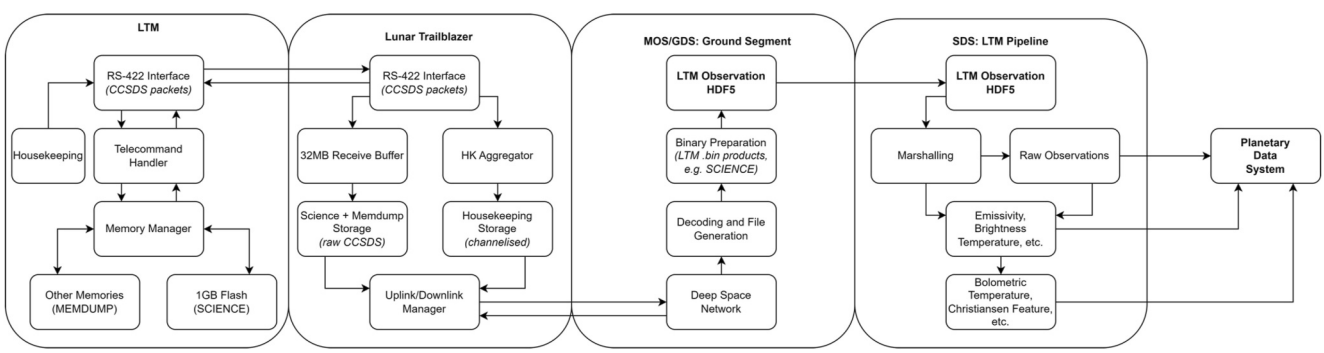

Figure 13. Data flow from the Lunar Thermal Mapper instrument through the ground data system and into the science data system.

Figure 14. Calibration pipeline used to generate the level 1 and higher products for the Planetary Data System (PDS).

BTM: Calibrated brightness temperature data in units of Kelvin ("BTM") (note: the derived surface temperature "TMP" is found in the "DER" directory).

EMS: Calibrated surface emissivity (unitless, 0 to 1; "EMS") provided both unprojected and map projected.

DER: Derived products. (a) Derived surface temperature in units of Kelvin ("TMP"); (b) Channel or channel ratio parameters indicative of surface composition ("PRM"). Products are provided both unprojected and map projected.

Initially unprojected products are provided; this will be updated as the in-flight geometric calibration and co-alignment with the HVM3 instrument (e.g., Gauld et al., 2025) is completed.

7. Conclusions

The LTM instrument was designed, assembled and calibrated to meet all its operational and scientific requirements for temperature and surface composition. The instrument was installed on the Lunar Trailblazer

spacecraft in February 2023 and launched in February 2025. Only limited telemetry from the instrument was received as the Trailblazer spacecraft was powered up, and these showed that the LTM was drawing the correct power, transitioned from boot to application software and the pointing mirror was in the Sun safe position. The mission was declared lost in July 2025.

Conflict of Interest

The authors declare no conflicts of interest relevant to this study.

Availability Statement

Software Availability Statement: Software archived in a repository: Software archived in a repository: Software used in the generation of the LTM radiometric model (Figure 11) is archived in the Oxford Research Archive (ORA) https://ora.ox.ac.uk. The code will be deposited at the ORA once this article is accepted, and this will generate an associated DOI. The calibration pipeline code is publicly available at https://github.com/namrah-habib/ltm-calibration-pipeline.

Data availability Statement: Data archived in a repository: Data used in the calibration of the LTM instrument (Figure 12) is archived in the Oxford Research Archive (ORA) https://ora.ox.ac.uk and the data (Bowles et al., 2025) is available at http://doi.org/10.5287/ora-5zpneea1q.

Acknowledgments
The LTM instrument was developed at the Department of Physics, University of Oxford under a grant from the UK Space Agency (UKSA, ST/W000415/1) and U.S. portions of this work were carried out under NASA contract 80MSFC19C0042. A portion of this research was carried out at the Jet Propulsion Laboratory, California Institute of Technology, under a contract with the National Aeronautics and Space Administration (80NM0019F0079). We thank all members of the Trailblazer and UKSA teams for their help and support throughout the development of the LTM instrument. At the UKSA we thank Lauren Taylor and Mamatha Maheshwarappa for their support throughout the project and with the recovery effort. Our thanks also go to the Matt Cosby and the team at Goonhilly Earth Station, UK, for their support during the recovery effort.

References

Arnold, J., Glotch, T. D., Lucey, P. G., Song, E., Thomas, I. R., Bowles, N. E., & Greenhagen, B. T. (2016). Constraints on olivine-rich rock types on the moon as observed by diviner and M3: Implications for the formation of the lunar crust. *Journal of Geophysical Research: Planets*, *121*(7), 1342–1361. https://doi.org/10.1002/2015je004874

Bandfield, J. L., Ghent, R. R., Vasavada, A. R., Paige, D. A., Lawrence, S. J., & Robinson, M. S. (2011). Lunar surface rock abundance and regolith fines temperatures derived from LRO diviner radiometer data. *Journal of Geophysical Research*, *116*, E00H02. https://doi.org/10.1029/2011JE003866

Bandfield, J. L., Poston, M. J., Klima, R. L., & Edwards, C. S. (2018). Widespread distribution of OH/H2O on the lunar surface inferred from spectral data. *Nature Geoscience*, *11*(3), 173–177. https://doi.org/10.1038/s41561-018-0065-0

Bowles, N. E., Ehlmann, B. L., Evans, R., Warren, T., Eshbaugh, H. H., King, G., & Woodward, S. (2025). LTM calibration data archive. *Authorea Preprints*. https://doi.org/10.5287/ora-5zpneea1q

Braden, S., Stopar, J., Robinson, M., Lawrence, S., Van Der Bogert, C., & Hiesinger, H. (2014). Evidence for basaltic volcanism on the moon within the past 100 million years. *Nature Geoscience*, *7*(11), 787–791. https://doi.org/10.1038/ngeo2252

Conel, J. E. (1969). Infrared emissivities of silicates: Experimental results and a cloudy atmosphere model of Spectral emission from condensed particulate mediums. *Journal of Geophysical Research*, *74*(6), 1614–1634. https://doi.org/10.1029/JB074i006p01614

Ehlmann et al., 2025 Ehlmann, B., et al. (2025). https://doi.org/10.1029/2025JE009300

Evans, R., Warren, T. J., et al. (2024). Design and testing of the lunar thermal mapper optics, proceedings of the SPIE, 13092, space telescopes and instrumentation 2024. *Optical, Infrared, and Millimeter Wave*, 130922K. https://doi.org/10.1117/12.3018436

Gauld, K. D., Dickson, J. L., Warren, T. J., Yang, J., Bowles, N., & Ehlmann, B. L. (2025). Post-acquisition image-based localization for high resolution thermal and visible/shortwave infrared images with application to the lunar trailblazer mission. *Earth and Space Science*, *13*(5), e2025EA004594. https://doi.org/10.1029/2025EA004594

Glotch, T. D., Lucey, P. G., Bandfield, J. L., Greenhagen, B. T., Thomas, I. R., Elphic, R. C., et al. (2010). Highly silicic compositions on the moon. *Science*, *329*(5998), 1510–1513. https://doi.org/10.1126/science.1192148

Greenhagen, B. T., Lucey, P. G., Wyatt, M. B., Glotch, T. D., Allen, C. C., Arnold, J. A., et al. (2010). Global silicate mineralogy of the moon from the diviner lunar radiometer. *Science*, *329*(5998), 1507–1509. https://doi.org/10.1126/science.1192196

Hayne, P. O., Aharonson, O., & Schorghofer, N. (2021). Micro cold traps on the moon. *Nature Astronomy*, *5*(2), 169–175. https://doi.org/10.1038/s41550-020-1198-9

Jaeger, J., & Harper, A. (1950). Nature of the surface of the moon. *Nature*, *166*(4233), 1026. https://doi.org/10.1038/1661026a0

Jolliff, B., Wiseman, S., Lawrence, S., Tran, T. N., Robinson, M. S., Sato, H., et al. (2011). Non-mare silicic volcanism on the lunar farside at Compton–Belkovich. *Nature Geoscience*, *4*(8), 566–571. https://doi.org/10.1038/ngeo1212

Laferriere, K. L., Sunshine, J. M., & Feaga, L. M. (2022). Variability of hydration across the southern hemisphere of the Moon as observed by deep impact. *Journal of Geophysical Research: Planets*, *127*(8), e2022JE007361. https://doi.org/10.1029/2022JE007361

Lawson, S. L., Jakosky, B. M., Park, H.-S., & Mellon, M. T. (2000). Brightness temperatures of the lunar surface: Calibration and global analysis of the clementine long-wave infrared camera data. *Journal of Geophysical Research*, *105*(E2), 4273–4290. https://doi.org/10.1029/1999JE001047

Mendell, W. W. (1976). [Ph.D. Thesis]. Rice University.

Mendell, W. W., & Low, F. J. (1974). Preliminary results of the apollo 17 infrared scanning radiometer. *The Moon*, *9*(1–2), 97–103. https://doi.org/10.1007/BF00565396

Murcray, F. H., Murcray, D. G., & Williams, W. J. (1970). Infrared emissivity of lunar surface features: 1. Balloon-borne observations. *Journal of Geophysical Research*, *75*(14), 2662–2669. https://doi.org/10.1029/JB075i014p02662

Murray, B. C., & Wildey, M. J. (1964). Surface temperature variations during the lunar nighttime. *The Astrophysical Journal*, *139*, 734–750. https://doi.org/10.1086/147799

Paige, D. A., Foote, M. C., Greenhagen, B. T., Schofield, J. T., Calcutt, S., Vasavada, A. R., et al. (2010a). The lunar reconnaissance orbiter diviner lunar radiometer experiment space science review. *Space Science Reviews*, *150*(1–4), 125–160. https://doi.org/10.1007/s11214-009-9529-2

Paige, D. A., Siegler, M. A., Zhang, J. A., Hayne, P. O., Foote, E. J., Bennett, K. A., et al. (2010). Diviner lunar radiometer observations of cold traps in the Moon's south polar region. *science*, *330*(6003), 479–482. https://doi.org/10.1126/science.1187726

Pettit, E., & Nicholson, S. B. (1930). Lunar radiation and temperatures. *The Astrophysical Journal*, *71*, 102–135. https://doi.org/10.1086/143236

Pieters, C. M., Hanna, K. D., Cheek, L., Dhingra, D., Prissel, T., Jackson, C., et al. (2014). The Second Conference on the Lunar Highlands Crust and New Directions. The distribution of Mg-spinel across the Moon and constraints on crustal origin. *American Mineralogist*, *99*(10), 1893–1910. https://doi.org/10.2138/am-2014-4776

Salisbury, J. W., Vincent, R. K., Logan, L. M., & Hunt, G. R. (1970). Infrared emissivity of lunar surface features: 2. Interpretation. *Journal of Geophysical Research*, *75*(14), 2671–2682. https://doi.org/10.1029/JB075i014p02671

Schorghofer, N., & Williams, J.-P. (2020). Mapping of ice storage processes on the moon with time-dependent temperatures. *The Planetary Science Journal*, *1*(3), 54. https://doi.org/10.3847/psj/abb6ff

Shirley et al., 2025 Shirley, K., et al. (2025). https://doi.org/10.1029/2025EA004590

Sunshine, J. M., Farnham, T. L., Feaga, L. M., Groussin, O., Merlin, F., Milliken, R. E., & A'Hearn, M. F. (2009). Temporal and spatial variability of lunar hydration as observed by the deep impact spacecraft. *Science*, *326*(5952), 565–568. https://doi.org/10.1126/science.1179788

Thompson, D., Ehlmann, B., Green, R., Allen, G., Bender, H., Copley-Woods, D., et al. (2026). Calibration and Performance of the High Resolution Volatiles and Minerals Moon Mapper (HVM) on Lunar Trailblazer. *Earth and Space Science*, *13*. https://doi.org/10.1029/2025EA004456

Williams, J.-P., Greenhagen, B. T., Paige, D. A., Schorghofer, N., Sefton-Nash, E., Hayne, P. O., et al. (2019). Seasonal polar temperatures on the moon. *Journal of Geophysical Research: Planets*, *124*(10), 2505–2521. https://doi.org/10.1029/2019JE006028

Yamamoto, S., Nakamura, R., Matsunaga, T., Ogawa, Y., Ishihara, Y., Morota, T., et al. (2010). Possible mantle origin of olivine around lunar impact basins detected by SELENE. *Nature Geoscience*, *3*(8), 533–536. https://doi.org/10.1038/ngeo897

Zhang, J. A., & Paige, D. A. (2009). Cold-trapped organic compounds at the poles of the moon and mercury: Implications for origins. *Geophysical Research Letters*, *36*(16), L16203. https://doi.org/10.1029/2009GL038614